

Ferromagnetic Properties of ZrZn_2

E. A. Yelland, S. J. C. Yates, O. Taylor, A. Grieths, S. M. Hayden and A. Carrington
 H. H. Wills Physics Laboratory, University of Bristol,
 Tyndall Avenue, Bristol BS8 1TL, United Kingdom
 (Dated: April 14, 2024)

The low Curie temperature ($T_C = 28\text{ K}$) and small ordered moment ($M_0 = 0.17\text{ }\mu_B\text{ f.u.}^{-1}$) of ZrZn_2 make it one of the few examples of a weak itinerant ferromagnet. We report results of susceptibility, magnetization, resistivity and specific heat measurements made on high-quality single crystals of ZrZn_2 . From magnetization scaling in the vicinity of T_C ($0.001 < |T - T_C| < 0.08$), we obtain the critical exponents $\beta = 0.52 \pm 0.05$ and $\gamma = 3.20 \pm 0.08$, and $T_C = 27.50 \pm 0.05\text{ K}$. Low-temperature magnetization measurements show that the easy axis is [111]. Resistivity measurements reveal an anomaly at T_C and a non-Fermi liquid temperature dependence $\rho(T) = \rho_0 + AT^n$, where $n = 1.67 \pm 0.02$, for $1 < T < 14\text{ K}$. The specific heat measurements show a mean-field-like anomaly at T_C . We compare our results to various theoretical models.

PACS numbers: 75.50.Cc, 74.70.Ad, 74.25.Fy, 74.70.-b

I. INTRODUCTION

Ferromagnetism in the cubic Laves compound ZrZn_2 was discovered by Matthias and Bozorth¹ in 1958. Its occurrence in ZrZn_2 is unusual because neither elemental Zr nor Zn is magnetically ordered. The low Curie temperature and small ordered moment of ZrZn_2 make it one of the few examples of a small-moment or weak itinerant ferromagnet. ZrZn_2 was initially considered to be a candidate for Stoner theory². However a quantitative comparison of Stoner theory with experiment suggests that spin fluctuation effects are important. In particular, the Curie temperature is strongly renormalized downwards from the Stoner value estimated from band structure parameters⁴.

ZrZn_2 crystallizes in the C15 cubic Laves structure shown in Fig. 1, with lattice constant $a = 7.393\text{ \AA}$. The Zr atoms form a tetrahedrally coordinated diamond structure and the magnetic properties of the compound derive from the Zr 4d orbitals, which have a significant direct overlap leading to the magnetic moment being spread out over the network shown by the thick lines in Fig. 1. ZrZn_2 is strongly unsaturated: an applied field of 5.7 T results in a 50% increase in the ordered moment. In contrast, strong ferromagnets such as Fe and Ni show a negligible increase of the ordered moment with field after a single domain is formed. The unsaturated behavior of ZrZn_2 indicates a large longitudinal susceptibility and the presence of longitudinal spin fluctuations^{5,6}. Further evidence for the existence of strong spin fluctuations in ZrZn_2 is provided by the remarkably large effective mass of its quasiparticles⁷. The low-temperature specific heat coefficient⁸ and the calculated DOS at the Fermi level⁷ imply an average mass enhancement $1 + \lambda = 5$ at zero applied magnetic field⁹. This is the largest known average mass enhancement for a d-band metal, and is even slightly larger than that of the strongly-correlated oxide system Sr_2RuO_4 for which $1 + \lambda = 3.6$ [Refs. 10, 11].

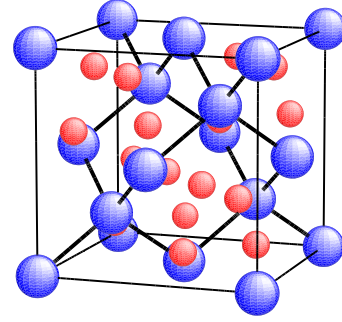


FIG. 1: (Color online) The C15 structure of ZrZn_2 . Zr atoms occupy the sites of the larger spheres.

It has been known for some time that the ferromagnetism of ZrZn_2 is extremely sensitive to pressure¹². Recent experiments on the samples studied here¹³ have shown that a pressure of $p_C = 16.5\text{ kbar}$ causes the ferromagnetism to disappear with a first order transition. Thus we may also view ZrZn_2 as being close to a quantum critical point (QCP)^{13,14}. In view of the strong longitudinal fluctuations present in ZrZn_2 and its proximity to a QCP, it has been proposed as a candidate for magnetically mediated superconductivity^{15,16,17,18}. However, as discussed elsewhere¹⁹, we find no evidence for bulk superconductivity at ambient pressure in these samples.

There are surprisingly few measurements of the fundamental properties of high-quality samples ($\text{RRR} \sim 100$) of ZrZn_2 in the literature. In this paper, we present a study of the transport and thermodynamic properties of ZrZn_2 . In particular, we have measured the magnetocrystalline anisotropy, the magnetization isotherms for $2 < T < 40\text{ K}$ and $0 < B < 5\text{ T}$; the resistivity from low temperatures through the Curie temperature; and the specific heat capacity for $0.3 < T < 40\text{ K}$. These

properties contain information about the quasiparticles and magnetic interactions in ZrZn_2 . For example, the temperature dependence of the resistivity at low temperatures gives information about the fundamental excitations that scatter quasiparticles, and the comparison of specific heat and magnetization data gives information about the importance of spin fluctuations in ZrZn_2 .

II. EXPERIMENTAL DETAILS

A. Crystal Growth and Sample Quality

ZrZn_2 melts congruently at 1180 C [Refs. 20,21]. At this temperature zinc has a vapor pressure of about 10 bars and is an aggressive flux. Thus we chose to grow ZrZn_2 by a directional cooling technique²². Stoichiometric quantities of high-purity zone-refined Zr (99.99%, Materials Research MARZ grade) and Zn (99.9999%, Metal Crystals) were loaded into a Y_2O_3 crucible. The total charge used was 4.2 g. The crucible was sealed inside a tantalum bomb which was closed by electron beam welding under vacuum. The assembly was heated to 1210 C and then cooled through the melting point at 2°C/hr^{-1} . The ingot was then annealed by cooling to 500 C over a period of 72 hr. This method produced, on occasions, single crystals of volumes up to approximately 0.4 cm^3 . Single crystals produced in this way had residual resistivities as low as $\rho_0 = 0.53\text{ m}\Omega$ corresponding to a residual resistance ratio $\text{RRR} = \rho(293\text{ K})/\rho(0) = 105$. With the exception of Ref. 23, previous reports by other groups of the fundamental transport and thermodynamic properties of ZrZn_2 have been carried out on samples with $\text{RRR} < 45$.

The residual resistivity ρ_0 and the Dingle temperature determined from de Haas-van Alphen measurements may be used to estimate the quasiparticle mean free path ℓ due to impurity scattering. For a crystal with cubic symmetry²⁴,

$$\ell = \frac{1}{4} \frac{e^2}{3} \frac{1}{\rho_0} \frac{1}{3} \sum_{\mathbf{F}} dS_{\mathbf{F}} = \frac{1}{4} \frac{e^2}{3} \frac{1}{\rho_0} \frac{1}{3} \sum_{\mathbf{F}} dS_{\mathbf{F}} : \quad (1)$$

From band structure calculations⁷, we estimate the sum of the Fermi surface areas to be $S_{\mathbf{F}} = 1.9 \times 10^{21}\text{ m}^2$. Hence $\ell_{\text{trans}} = 1350\text{ \AA}$. A second estimate of the quasiparticle mean free path can be made from the de Haas-van Alphen effect⁷; values are in the range $\ell_{\text{dHvA}} = 1500\text{--}2800\text{ \AA}$ depending on Fermi surface orbit, in approximate agreement with ℓ_{trans} . In general, one expects that $\ell_{\text{dHvA}} < \ell_{\text{trans}}$ since ℓ_{trans} is weighted towards large momentum changes²⁵, whereas ℓ_{dHvA} weights all scattering equally. However, the opposite situation $\ell_{\text{dHvA}} > \ell_{\text{trans}}$ may also arise in an inhomogeneous sample, since the exponential scattering rate dependence of the Dingle factor $R_D = \exp(-m_b/eB)$ causes ℓ_{dHvA} to be strongly weighted towards high quality regions of the sample. Given these considerations, the two mean free path es-

timates ℓ_{dHvA} and ℓ_{trans} are as consistent as can be expected.

B. Transport and Thermodynamic Measurements

Resistivity measurements were made using a standard a.c. technique using a Brookdeal 9433 low-noise transformer and SR850 digital lock-in amplifier with a measuring frequency $f = 2\text{ Hz}$. Sample contacts were made with DuPont 4929 conducting Ag/epoxy. Measurements of a.c. susceptibility were made by a standard technique in which the sample was mounted inside a small coil of approximately 2500 turns. The system was calibrated using the superconducting transition of an indium sample of similar size to the ZrZn_2 sample. Magnetization measurements were made using a commercial Quantum Design MPMS-XL SQUID magnetometer.

Heat capacity measurements were made both by a long-pulse method and an a.c. method²⁶. In the long-pulse technique²⁷ the sample was mounted on a silicon platform connected to a temperature-controlled stage by a thin copper wire. In the a.c. technique the sample was mounted on a flattened 12 m chromel-constantan thermocouple and heated optically. The long pulse technique allows an accurate determination of the absolute value of $C(T)$ but has relatively low resolution. The a.c. technique has much higher resolution ($< 0.1\%$), and is thus ideally suited to resolving the small anomaly at T_C . However, it does not allow an accurate determination of the absolute value of $C(T)$ due to the poorly defined addenda contribution. We estimated the addenda by measuring a Cu sample with similar $C(T)$; the a.c. data with the estimated addenda subtracted were multiplied by a scale factor to match the long-pulse data at a single temperature.

III. RESULTS

A. Magnetization Isotherms and Scaling near the Ferromagnetic Transition

1. Low Temperature Isotherms

Since the discovery of ZrZn_2 there have been many studies of the magnetic properties. Previous work^{1,12,18,23,28,29,30,31,32,33,34} has shown that the Curie temperature and the ordered moment, are strongly dependent on sample quality and composition²⁹. Thus the purpose of the present magnetization measurements is to attempt to characterize the magnetic properties in the clean limit. The high-quality of our samples is indicated by their low residual resistivity ($\text{RRR} = 105$) and long mean free path, which has allowed much of the Fermi surface to be observed by the dHvA effect⁷.

Although many plots of the magnetization isotherms for ZrZn_2 have been reported^{23,28,29,31} in improved instru-

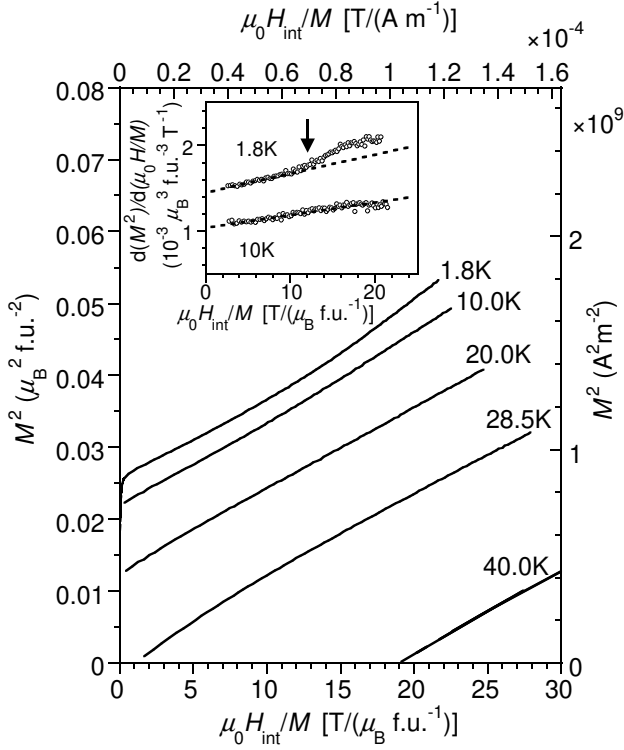


FIG. 2: Arrott plot of magnetization isotherms in the temperature range 1.8 K – 40 K. In the Stoner theory of a weak itinerant ferromagnet, M^2 is a linear function of $H \approx M$. Inset: the derivative $d(M^2)/d(\mu_0 H/M)$ of the 1.8 K and 10 K Arrott curves; the 1.8 K curve is offset by $+5 \times 10^{-3} \mu_B^2 \text{ f.u.}^{-2} \text{ T}^{-1}$. Dotted lines are guides to the eye. Note the feature in the 1.8 K curve, indicated by an arrow.

mentation and higher sample quality have recently allowed the structure to be observed. For a weak ferromagnet, the magnetization isotherms are generally expected to obey the Stoner form in which M^2 is a linear function of $H \approx M$. Fig. 2 is an Arrott plot of our magnetization isotherms. The near linearity of the isotherms confirms that they are indeed of approximately the expected form. However, the isotherm at $T = 1.8 \text{ K}$ shows an intriguing feature at $\mu_0 H = 2.4 \text{ T}$, indicated by an arrow in Fig. 2. Another more pronounced feature is directly visible in the $T = 1.75 \text{ K}$ $M(H)$ isotherm plotted in Ref. 18, at a field 6 T, outside the range of our present measurements. Structure in the electronic DOS close to the Fermi level is expected to have a profound influence on $M(T; B)$ in itinerant ferromagnets^{35,36}, and calculations⁷ suggest that just such structure is present in the DOS of ZrZn_2 , the Fermi level lying between two sharp peaks in the majority spin DOS. This is an interesting connection that could be explored in future work.

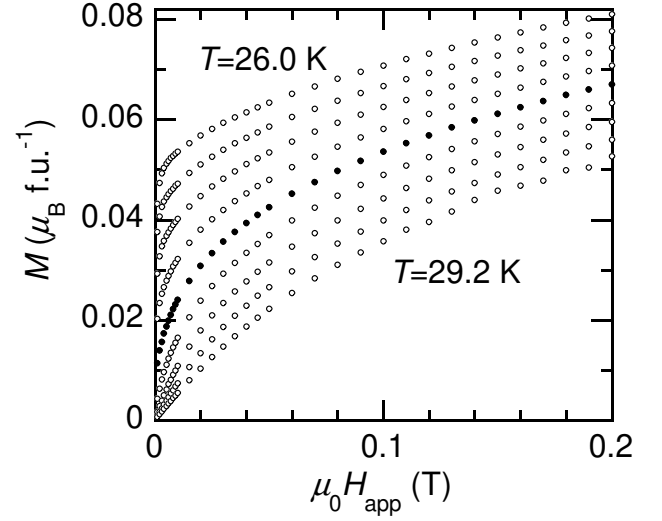


FIG. 3: Low field magnetization isotherms near the ferromagnetic critical temperature of ZrZn_2 (near-critical isotherm at $T = 27.6 \text{ K}$ shown by filled circles).

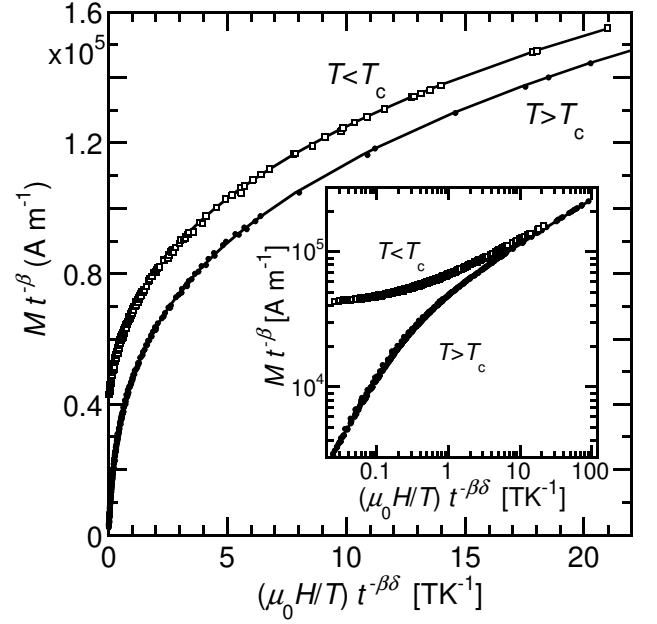


FIG. 4: Scaling plot of magnetization isotherms of ZrZn_2 near T_c . The data shown here are the same as those in Fig. 3 except that we have excluded the region $\mu_0 H < 0.005 \text{ T}$ to avoid systematic errors due to multiple ferromagnetic domains inside the sample (see text). The correct choice of T_c , and causes the scaled data to collapse onto a single curve for $T < T_c$ and another for $T > T_c$. The values that allow the best fit to the scaled data of a 7th order polynomial in M are shown in Table I. The solid lines show the best fit polynomials for $T < T_c$ and $T > T_c$. The inset shows the same data on log-log axes.

2. Scaling near T_c

At temperatures approaching the Curie temperature of a ferromagnet the magnetization isotherms $M(H)$ become highly nonlinear making the identification of T_c difficult. An accurate determination of T_c can be achieved by a scaling analysis of the magnetization close to the transition; we have therefore measured magnetization isotherms at a set of temperatures near T_c allowing us to determine T_c and the magnetization scaling exponents.

Close to the critical temperature of a ferromagnetic transition, the magnetization $M(H; T)$ can be expressed as $M(h)$ where $M = M/t$ and $h = (H - T)t$ are appropriately scaled quantities³⁷. Here $t = |T - T_c|$ is the reduced temperature and β, γ are the critical exponents. The experimental determination of β and γ allows remarkably universal conclusions to be drawn about the physical model which underlies the phase transition. We have measured the magnetization $M(H)$ in applied fields $0 < H < 0.2$ T at closely spaced temperatures in the range $0.1 \text{ K} \leq T \leq 2.2$ K. Fig. 3 shows the raw data. In order to determine T_c and the scaling exponents, M and h were calculated from the experimental data set for all values of T ; and T_c within a certain volume of the 3D parameter space encompassing both the Heisenberg and mean field models. For each combination of values, the polynomial in M which best fits the scaled experimental values of h was found, and its goodness-of-fit (χ^2) value calculated. The correct parameter values are taken as those for which the best fit polynomial has the lowest χ^2 . Only data points for which $H_{\text{app}} < 0.05$ T are included in the scaling analysis in order to ensure the formation of a single ferromagnetic domain inside the sample. The data have been corrected for the small demagnetizing factor of this sample, $D = 0.060$, but we note that the final results are barely affected by this. We find $T_c = (27.50 \pm 0.05)$ K, $\beta = 0.52 \pm 0.05$ and $\gamma = 3.20 \pm 0.08$ (see Table I). The values of β and γ are close to those obtained on lower quality samples with smaller T_c 's³³.

In order to interpret our scaling results, we need to know whether we are in the critical region. The Ginzburg criterion³⁸,

$$T_G = \frac{T_c k_B^2}{32 \pi^2 (C_V)^2 \epsilon_0} \quad (2)$$

allows us to estimate the extent of the critical region. From neutron scattering measurements³⁹ of the wavevector-dependent magnetic susceptibility $\chi(q)$ and low temperature magnetization measurements we estimate the magnetic correlation length $\xi_0 = 33$ Å. The specific heat jump is $C = 155 \text{ mJ K}^{-1} \text{ mol}^{-1}$ (see section IIID). Hence $T_G = 0.4 \text{ mK}$. Thus our data are collected outside the critical region where mean field behavior is expected. Table I shows that our results are indeed in agreement with the expected mean field results for a 3D ferromagnet. Finally, it is worth commenting that determining the Curie temperature T_c from critical scaling,

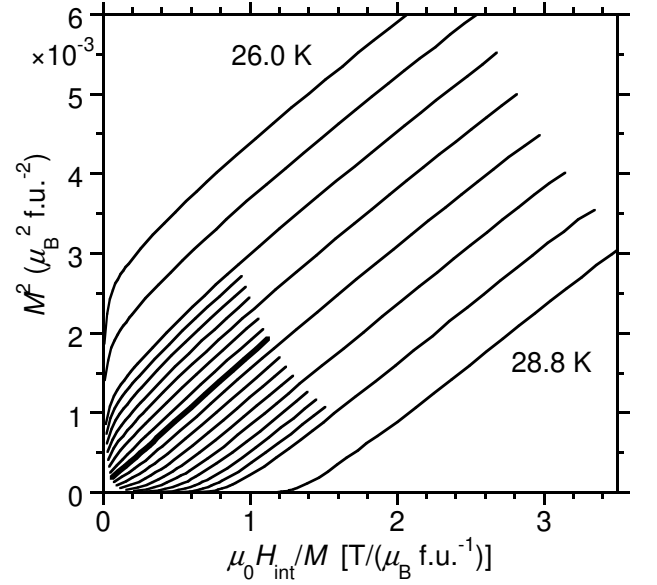


FIG. 5: A plot of magnetization isotherms near T_c for ZrZn_2 . The isotherms were measured at 0.4 K intervals and at 0.1 K intervals close to T_c ; the bold line is the critical isotherm at $T = 27.5$ K. In the Stoner theory of a weak itinerant ferromagnet, M^2 is a linear function of $H = M$.

TABLE I: Theoretical critical exponents for various models of phase transition and the experimental values found in this work. T_c was found to be 27.50 ± 0.05 K.

| | mean-field | Heisenberg | this work |
|----------|------------|------------|-----------------|
| β | 0.5 | 0.326 | 0.52 ± 0.05 |
| γ | 3 | 4.78 | 3.20 ± 0.08 |

as described here, yields a lower value than that obtained by taking the peak in (dM/dB) with T . This may explain the slightly higher values reported elsewhere¹⁸ for similar samples.

B. Magnetocrystalline Anisotropy

The exchange interaction in an itinerant electron system is often modelled as isotropic, depending only on the relative orientation of electron spins. However, the crystal field also enters the free energy via spin-orbit coupling, causing anisotropy of magnetic properties. One motivation for studying the magnetocrystalline anisotropy is that it has implications for the symmetry of the superconducting order parameter in the spontaneous mixed state of the putative superconducting phase of ZrZn_2 [Ref. 40].

Fig. 7 shows a low-field hysteresis loop measured for applied fields in the range $0.05 \text{ T} < H_{\text{app}} < 0.05 \text{ T}$. The main panel shows that a field of approximately 5 mT is sufficient to create a single ferromagnetic domain. The inset reveals the low coercive field of the present samples

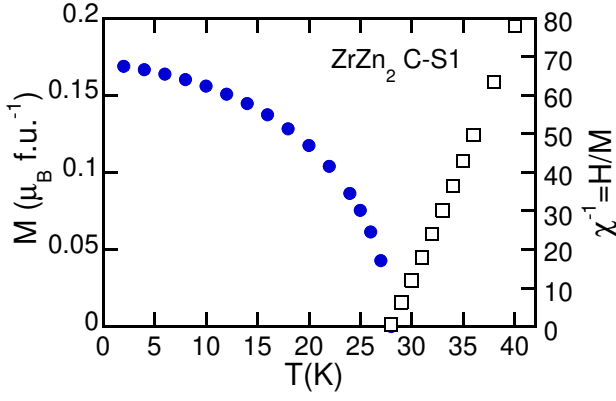


FIG. 6: The temperature dependence of the magnetization (filled circles) and the inverse susceptibility (open squares) as determined from Arrott plots.

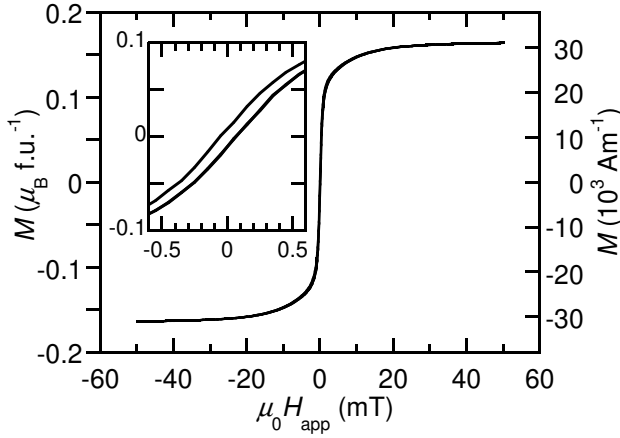


FIG. 7: Magnetic hysteresis curve for ZrZn_2 measured at $T = 5\text{ K}$. The inset shows the central region magnified. Note the small coercive field $H_{\text{coer}} = 0.05\text{ mT}$.

$H_{\text{coer}} = 0.05\text{ mT}$ and justifies our method (see below) for obtaining the magnetic anisotropy constants.

We have determined the ferromagnetic anisotropy of ZrZn_2 from $M(H)$ isotherms at $T = 5\text{ K}$. A disc-shaped sample (diameter $2R = 2.72\text{ mm}$, thickness $t = 0.47\text{ mm}$) was spark-cut so that the plane of the disc was (110) . This geometry allows access to the three major cubic symmetry directions $[100]$, $[110]$ and $[111]$ with the magnetic field in the plane of the disc so that the demagnetizing field is the same in each orientation. For this sample, the volume averaged demagnetizing factor is $D = 0.146$ [Ref. 41], which for $M = 0.16\text{ B f.u.}^{-1}$ corresponds to an average demagnetizing field $\mu_0 H_D = 0.037\text{ T}$ inside the sample. In this section we denote the measured magnetization by M_k to emphasize that the SQUID measurement is only sensitive to the component of M parallel to H_{app} , which is vital for extracting the anisotropy constants by the thermodynamic method described later. Fig. 8 shows $M_k(H_{\text{int}})$ measured with H_{app} parallel to each of the

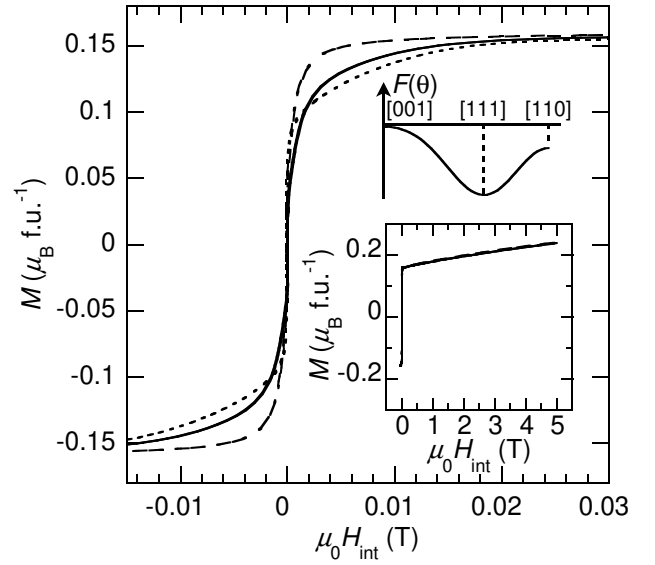


FIG. 8: Magnetization curves of a ZrZn_2 single crystal measured at $T = 5\text{ K}$ with field applied along $[100]$ (dotted line), $[110]$ (solid line) and $[111]$ (dashed line). The ferromagnetic easy axis is seen to be $[111]$ at this temperature. Upper inset: plot of Eq.(2) using values of K_1 and K_2 determined from $M_k(H_{\text{int}})$ as described in the text. Lower inset: $M_k(H_{\text{int}})$ up to 5 T for the same sample.

three symmetry directions; H_{int} is the internal field that, in a simple scalar notation, is approximately related to the applied field H_{app} by $H_{\text{int}} = H_{\text{app}} - DM$. As H_{int} increases from zero, a single domain is rapidly formed. The slower increase in $M_k(H_{\text{int}})$ for $\mu_0 H_{\text{int}} > 0.003\text{ T}$ with H_{app} $\parallel [001]$ or $[110]$, arises from the rotation of M away from the easy axis towards H_{int} as the ratio of the interaction term $M \cdot H_{\text{int}}$ to the anisotropy energy increases. Fig. 8 shows that saturation is reached most rapidly with H_{app} $\parallel [111]$, demonstrating that $[111]$ is the ferromagnetic easy axis at this temperature.

The principal cause of the rounding of the $M_k(H_{\text{int}})$ curve, even for $H \parallel [111]$, is likely to be the inhomogeneity of the demagnetizing field. The only practical sample shapes that give a uniform demagnetizing field are ellipsoids of revolution. We have calculated the volume distribution of the demagnetizing field for a perfect cylinder of the required aspect ratio assuming that the magnetization is uniform; the characteristic width of the distribution is $D = 0.07$ and, for example, 12% of the sample volume has a local demagnetizing field that exceeds the volume average value by a factor > 1.5 . Angular misalignments of up to 2° may also contribute.

The first two terms in the standard expansion of the anisotropic free energy of a ferromagnet with cubic symmetry⁴² can be expressed, for the present geometry,

as

$$F(\theta) = \sin^2(\cos^2\theta + \frac{1}{4}\sin^2\theta)K_1 + \frac{1}{4}(\sin^4\theta - \cos^2\theta)K_2 \quad (3)$$

where θ is the angle within the (110) plane between M and [100] and $K_{1,2}$ are the first and second anisotropy constants. It is possible, in principle, to determine the anisotropy constants by assuming that M is fixed in the 'approach to saturation' region of the $M_k(H_{\text{int}})$ curve⁴². In this picture, the direction of M (and hence the magnitude of M_k) for any given H_{int} is determined from the condition that the torque acting on M due to the anisotropy exactly balances the torque due to the interaction of M with H_{int} . However we choose an alternative thermodynamic method⁴² to extract anisotropy constants from $M(H)$ which is less reliant on assumptions about the demagnetizing field. We calculate the total magnetic work done in order to bring the sample to saturation with H_{app} applied parallel to a certain crystal direction. The work required to produce an infinitesimal increase, dm , in the sample moment is $dW = \mu_0 H_{\text{app}} dm$. Since the irreversibility of $M(H)$ is negligible in ZrZn_2 , we can relate the magnetic work done to a change in the appropriate thermodynamic function of state, namely the Gibbs free energy, and we obtain $G = \mu_0 H_{\text{app}} dm$. The anisotropy energy $F(\theta)$ is therefore given (apart from an irrelevant constant) by the area under the $H_{\text{app}}(M_k)$ curve. From Eq. (2) it follows that $K_1 = 4(F_{[110]} - F_{[001]})$ and $K_2 = 9(F_{[001]} + 3F_{[111]} - 4F_{[110]})$. Evaluating the areas corresponding to the magnetic work, we find $F_{[110]} - F_{[111]} = 1.1 \times 10^8 \text{ eV fm}^{-1}$ and $F_{[001]} - F_{[111]} = 1.6 \times 10^8 \text{ eV fm}^{-1}$. The cubic anisotropy constants are therefore $K_1 = 2.0 \times 10^8 \text{ eV fm}^{-1}$, $K_2 = 2.6 \times 10^7 \text{ eV fm}^{-1}$. The magnitude of the ferromagnetic anisotropy is therefore a factor 3 smaller than that found in the weak itinerant ferromagnet Ni_2Al [Ref. 43] ($1 \text{ erg cm}^{-3} = 3.15 \times 10^{11} \text{ eV fm}^{-1}$ in ZrZn_2), where the relative sizes of K_1 and K_2 are opposite to those in ZrZn_2 , and almost two orders of magnitude smaller than in Ni [Ref. 44].

The magnetocrystalline anisotropy of ferromagnetic metals can in principle be obtained from band-structure calculations of the total energy in which the effect of spin-orbit coupling is included^{45,46}. It would be interesting to see whether such calculations correctly predict the magnetic anisotropy of ZrZn_2 .

C. Resistivity

Many systems close to a quantum critical point have been shown to exhibit a so-called non-Fermi liquid temperature dependence of the resistivity. Non-Fermi liquid is generally accepted to mean that the low temperature exponent n in the equation $\rho(T) = \rho_0 + AT^n$ is not equal to 2. Notable examples of systems exhibiting non-Fermi liquid power laws in the resistivity include

high-temperature superconductors ($n \rightarrow 1$ close to optimal doping), heavy Fermion antiferromagnets, such as CePd_2Si_2 [Ref. 47] ($n \rightarrow 1.2$ at high pressure close to quantum criticality), and the helical ferromagnet MnSi [Ref. 48] ($n \rightarrow \frac{5}{3}$ as $T \rightarrow 0$, in the paramagnetic state close to the pressure-induced ferromagnet-paramagnet QPT). The low moment ferromagnets Ni_2Al and YNi_2 ($M(0,0) = 0.075$ and $0.04 \mu_B \text{ f.u.}^{-1}$ respectively) exhibit a non-Fermi liquid resistivity over a wider range of pressures about the QCP and, even at ambient pressure, a $T^{1.65}$ dependence is observed over a small temperature range⁴⁹.

Fig. 9 shows the temperature dependence of the resistivity for ZrZn_2 . On cooling the sample through T_C , we observe a slight 'kink' in the resistivity near the Curie temperature. Similar behavior is observed in other itinerant ferromagnets such as nickel, although the behavior in ZrZn_2 is not as pronounced as that in stronger ferromagnets. The resistivity anomaly associated with the ferromagnetic transition can be emphasized if a background variation of the form $\rho_0 + AT^2$ is subtracted from the data; the result is shown in the lower inset. It has been argued that the dominant magnetic contribution to the resistivity is due to short range spin fluctuations and therefore $d\rho/dT$ should vary like the magnetic specific heat near the critical point⁵⁰. To test this hypothesis we have plotted $d\rho/dT$ in the upper inset of Fig. 9. There is good qualitative agreement with the measured specific heat anomaly (see inset to Fig. 10).

At lower temperatures, in the ferromagnetic state, the resistivity has a well defined non-Fermi liquid behavior. Fitting data over the temperature range $1 < T < 14 \text{ K}$, we find $n = 1.67 \pm 0.02$. The inset to Fig. 9 shows that when ρ is plotted against $T^{5/3}$, a linear behavior is obtained up to about 15 K. The existence of a $T^{5/3}$ power law very close to the ferromagnetic QCP has already been established in high-pressure measurements on ZrZn_2 [Ref. 32] but our result shows that the unusual power law applies well away from the QCP. Early data on a polycrystalline sample³⁰ showed a $T^{5/3}$ temperature dependence in the range $15 < T < 50 \text{ K}$ but notably not at lower temperatures.

It has been pointed out by a number of workers that a $\rho/T^{5/3}$ behavior may be understood in terms of scattering of quasiparticles by spin fluctuations⁵¹. A $T^{5/3}$ dependence is expected near a 3D ferromagnetic quantum critical point where the collective spin excitations are expected to be overdamped. Thus it appears that ZrZn_2 is sufficiently close to quantum criticality to observe the $5/3$ non-Fermi liquid behavior.

It has been reported that ZrZn_2 displays superconductivity below about 0.6 K. We find no traces of superconductivity in our resistivity curves at ambient pressure in samples etched in a HF/HNO_3 solution¹⁹.

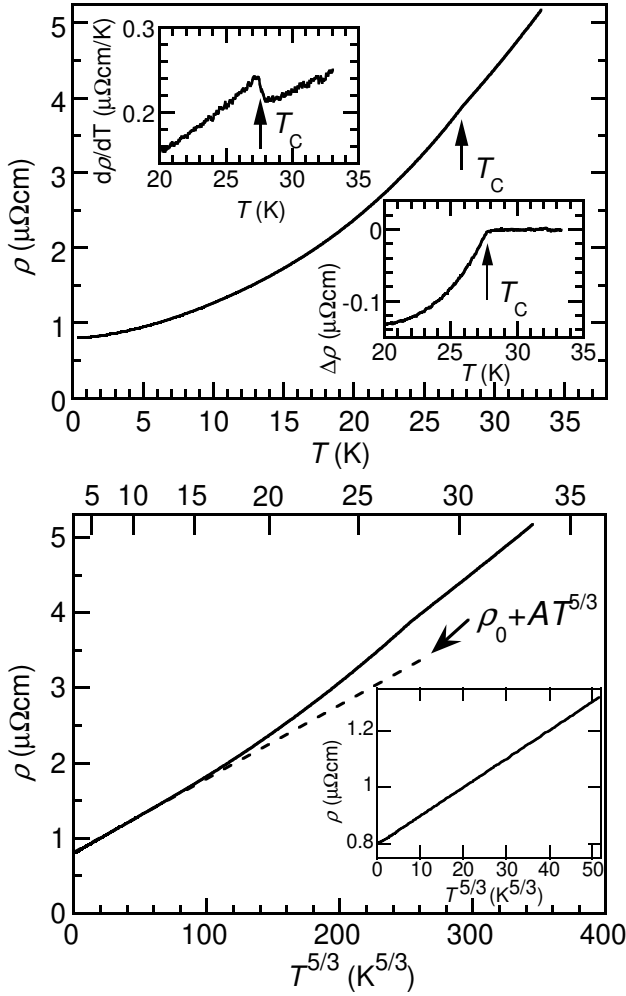


FIG. 9: Upper panel: raw $\rho(T)$ results for $0.5 < T < 32$ K; upper inset: $d\rho/dT$ close to T_C ; lower inset: $\rho(T)$ results close to T_C after subtraction of a smoothly varying background (see text). Lower panel: $\rho(T)$ plotted against $T^{5/3}$; inset: the same data over a limited T range, demonstrating the non-Fermi liquid power law $\rho(T) = \rho_0 + AT^{5/3}$.

D. Heat Capacity

Fig. 10 shows specific heat results for $T < 40$ K on single crystal samples that were cut from a region of the ingot next to that used for resistivity measurements. As with previous measurements⁸ a large linear contribution to the specific heat $C = \gamma T$ was observed at low temperatures, with $\gamma = 45 \text{ mJ K}^{-2} \text{ mol}^{-1}$. At higher temperatures the high-sensitivity of a.c. specific heat measurements allows the small ferromagnetic anomaly to be observed.

The anomaly in $C(T)$ at the ferromagnetic transition is only 2.5% of the total in ZrZn_2 ; a reliable separation of the magnetic heat capacity C_m therefore means that both the electronic and phonon components must be determined precisely, and this is not a trivial task. In order

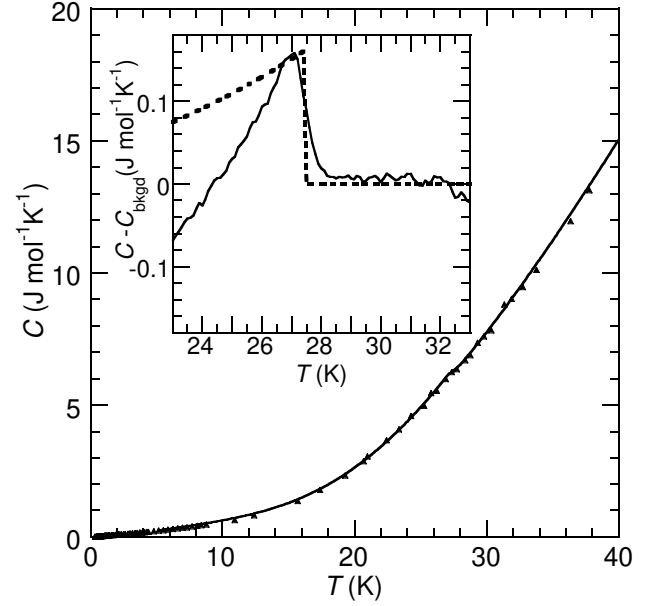


FIG. 10: Specific heat $C(T)$ of single crystal ZrZn_2 : symbols show data obtained using a pulse-relaxation technique; solid line shows the results obtained by a high sensitivity a.c. method. Inset: solid line shows a.c. data close to T_C after subtracting a smoothly varying background (see text); dashed line shows $C_m(T)$ calculated by Stoner theory, multiplied by a scale factor 0.5.

to emphasize the ferromagnetic anomaly, in the inset to Fig. 10 we have plotted the heat capacity after subtracting a smoothly varying estimate of the non-magnetic heat capacity of the form $C_{\text{bkgd}}(T) = \gamma T + C_{\text{Debye}}(T)$; here C_{Debye} is the Debye heat capacity function and γ is a Debye temperature. We set $\gamma = 38 \text{ mJ K}^{-2} \text{ mol}^{-1}$, close to that observed at low temperatures, in order to obtain a fit to $C_m(T)$ immediately above T_C ; the only other free parameter was allowed to vary to give the best fit to the data in a small temperature range $29 < T < 33$ K above T_C , giving a value $\gamma = 284 \text{ K}$. We emphasize that this estimate of the non-magnetic heat capacity may not be correct in detail (e.g. there may be significant fluctuation heat capacity in the range of the fit and we have not taken into account the true phonon DOS), but our quantitative discussion will be confined to the height of the discontinuity at T_C which is hardly affected by the choice of background.

The jump in C at T_C measured here is about a factor of 2 larger than that measured previously⁵² on a sample with $T_C = 10$ K. The shape of the anomaly, shown in the inset to Fig. 10, broadly resembles that expected for a mean-field second order transition. However, closer inspection shows that there is curvature in our estimate of $C_m(T)$, both above and below the jump at T_C , up to 1.5 K from T_C . This almost certainly results from thermal fluctuations, although our uncertainty in the background precludes a detailed analysis. There is also evi-

dence of some rounding of the anomaly from sample inhomogeneity on a smaller temperature scale $\sim 0.2\text{ K}$.

We now compare our results with Landau and spin fluctuation theories. In the Landau approach, the free energy is written in the form

$$F = \frac{1}{2}a(T)M^2 + \frac{1}{4}bM^4 - MB : \quad (4)$$

First, we relate the parameters of the theory, namely the Landau coefficients $a(T)$ and b , to experimental quantities determined near T_C . In mean field theory one usually assumes that the coefficient $a(T)$ varies linearly with temperature near T_C so that $a(T) = \underline{a}t$, where $t = (T - T_C)/T_C$. By minimizing the Landau free energy Eq. 4 with $B = 0$, we find the spontaneous magnetization is

$$M = \sqrt{\frac{\underline{a}t}{b}} : \quad (5)$$

Combining Eq. 4 and Eq. 5, the zero-field specific heat can be evaluated from the thermodynamic relation $C_V = T(d^2F/dT^2)$,

$$C_m^{(\text{Landau})} = \frac{\underline{a}^2 T}{2bT_C^2} \quad \text{for } T < T_C ; \\ = 0 \quad \text{for } T > T_C : \quad (6)$$

Since this simple model only includes terms in the free energy that are dependent on the macroscopically ordered moment, C_m must vanish above T_C ; the discontinuity in the specific heat at T_C is simply the limiting value as $T \rightarrow T_C$, i.e. $C_m = \underline{a}^2/2bT_C$. This value can easily be compared with experiment by noting that the gradient of the critical isotherm in the Arrott plot Fig. 2 gives $\underline{a}=b$ and that in the magnetization scaling plot Fig. 4, the intercept of the $T < T_C$ data with the ordinate axis gives $\underline{a}=b$ directly. From the data we obtain $b = 1.1 \cdot 10^{13} \text{ T (Am}^{-1}\text{)}^3$ and $\underline{a}=b = 4.0 \cdot 10^4 \text{ Am}^{-1}$. This gives a discontinuity $C_m^{(\text{Landau})} = 150 \text{ m JK}^{-1} \text{ mol}^{-1}$, in excellent agreement with the experimental value of $155 \pm 30 \text{ m JK}^{-1} \text{ mol}^{-1}$. The agreement between our measured C and that calculated from the magnetization isotherm provides a consistency check on the Landau theory.

The specific heat anomaly in weak itinerant ferromagnets has been the subject of various theoretical studies^{53,54,55,56,57,58}. In the Stoner-Wohlfarth model⁵³, the Landau coefficient a has the temperature dependence

$$a(T) = \frac{0}{2} + 1 \frac{T^2}{T_C^2} ; \quad (7)$$

In this model the exchange field is proportional to the magnetization; the T dependence of a reflects the reduction in magnetization due to thermal spin-flipping excitations. The b coefficient can be obtained by minimizing

F at $T = 0$, giving

$$b = \frac{0}{2} \frac{M_0^2}{M_0^2} ; \quad (8)$$

where

$$0 = \frac{dM}{dB} \Big|_{B,T=0} ; \quad (9)$$

and M_0 is the $T = 0$ magnetization. As in the Landau model, we can estimate the specific heat from $F(T)$ [Ref. 53],

$$C_m^{(\text{Stoner})} = \frac{M_0^2}{2} \frac{T}{T_C} - 3 \frac{T^3}{T_C^3} \quad \text{for } T < T_C ; \\ = 0 \quad \text{for } T > T_C : (10)$$

Using $M_0 = 3.1 \cdot 10^4 \text{ Am}^{-1}$ (0.17 B fu.^{-1}) and $0 = 4.2 \cdot 10^3$, as determined from $M(H)$ measurements at $T = 1.8\text{ K}$ [Ref. 18], we find $C_m^{(\text{Stoner})} = 330 \text{ m JK}^{-1} \text{ mol}^{-1}$ which is a factor 2 larger than the experimental value.

The Stoner-Wohlfarth approach can only include the effect of spin fluctuations through the renormalization of its phenomenological parameters. Experiments have shown that many of the properties of weakly ferromagnetic materials such as ZrZn_2 and Ni_2Al cannot be explained within this framework. Perhaps the most obvious property not explained by a mean field approach is the temperature dependence of the susceptibility above T_C , for which experiment shows a Curie-Weiss dependence $\propto (T - T_C)^{-1}$ as opposed to the $\propto (T - T_C)^{-2}$ predicted by Stoner theory. In order to address the deficiencies of mean field theories, various self-consistent renormalized (SCR) spin fluctuation models have been proposed^{3,5,6}. These follow the Landau-Ginzburg approach and treat the local magnetization $m(r)$ as a fluctuating stochastic variable. The SCR theory allows both magnetic corrections above T_C and the renormalizing effect of spin fluctuations on the Landau parameter to be taken into account. The effect of including spin fluctuations is to reduce the discontinuity in the specific heat C_m at T_C . This has been estimated by Mohn and Hilscher⁵⁵ based on the model of Murata and Doniach⁵,

$$C_m^{(\text{SCR})} = \frac{0 M_0^2}{4} \frac{1}{T_C} : \quad (11)$$

Note that the Mohn and Hilscher value $C_m^{(\text{SCR})} = (1/4) C_m^{(\text{Stoner})}$. The experimental value of C_m and the various model predictions are summarized in Table II.

In summary, the Stoner-Wohlfarth model overestimates the specific heat jump and the SCR theory, as implemented in Refs.^{5,55}, underestimates the jump. It is pleasing to note however that the shape of the anomaly predicted by Stoner theory is similar to that observed experimentally. Because of the nature of the theories one cannot attribute their failure to a single approximation.

TABLE II: Comparison of calculated and measured specific heat discontinuities.

| | Landau | Stoner | SCR | Exp |
|---|--------|--------|-------|-------|
| C (mJ K ⁻¹ mol ⁻¹) | 0.15 | 0.33 | 0.081 | 0.155 |

In the case of the Stoner theory the phenomenological parameters (T_C , γ_0 , b) used as inputs to the model are not taken directly from band structure calculations, rather they are determined from the experimental magnetization $M(B; T)$ and thus can be renormalized by fluctuations. The fact that the Stoner-Wohlfarth theory overestimates the specific heat jump suggests that paramagnetic correlations give a significant contribution to the specific heat above T_C . The SCR-theory might be improved by using a more realistic model for the excitations ($\chi(q; \omega)$) below T_C , where the longitudinal and transverse excitations are treated separately. Unfortunately, a full implementation of the SCR theory including, for example, the effects of the changes in the magnetic excitation spectrum on entering the ferromagnetic state is difficult⁶.

E. Conclusion

In conclusion we have studied various thermodynamic and transport properties of the weak itinerant ferromagnet

net ZrZn_2 . Magnetization measurements show that the easy crystallographic axis is [111] and scaling plots reveal mean-field exponents for the temperature range studied. Specific heat measurements reveal an anomaly whose shape is reminiscent of mean-field behavior. However, the measured discontinuity is significantly smaller than that predicted by Stoner-Wohlfarth theory. The resistivity shows an anomaly at T_C and a non-Fermi liquid $T^{5/3}$ behavior at low temperatures. Our results demonstrate the importance of collective spin fluctuations in ZrZn_2 , a material that was once considered to be a candidate for a Stoner ferromagnet.

Acknowledgments

We wish to thank N.R. Bernhoeft, G.G. Lonzarich, P.J. Meeson, and C.P. Eiderer for informative discussions and help with this work, and C. Pitrou for performing some preliminary heat capacity experiments. The research has been supported by the EPSRC.

- ¹ B. T. M atthias and R. M. B. orth, Phys. Rev. 109, 604 (1958).
- ² E. C. Stoner, Proc. Roy. Soc. A 154, 656 (1936).
- ³ T. Mori, Spin Fluctuations in Itinerant Electron Magnetism (Springer-Verlag, Berlin, 1985).
- ⁴ J. Kubler, Phys. Rev. B 70, 064427 (2004).
- ⁵ K. K. Murata and S. Doniach, Phys. Rev. Lett. 29, 285 (1972).
- ⁶ G. G. Lonzarich and L. Taillefer, J. Phys. C 18, 4339 (1985).
- ⁷ S. J. C. Yates, G. Santi, S. M. Hayden, P. J. Meeson, and S. B. Dugdale, Phys. Rev. Lett. 90, 057003 (2003).
- ⁸ C. P. Eiderer, A. F. t, H. von Lohneysen, S. M. Hayden, and G. G. Lonzarich, J. Magn. Magn. Mater. 226-230, 258 (2001).
- ⁹ At a nite eld $B = 9$ T, de Haas-van Alphen measurements give quasiparticle masses that are enhanced above band-structure values by a factor 3{5, in good agreement with heat capacity measurements at this eld⁸ which suggest $1 + \gamma_0/3$.
- ¹⁰ A. P. M ackenzie, S. R. Julian, A. J. D iver, G. J. M cM ullan, M. P. Ray, G. G. Lonzarich, Y. M aeno, S. N ishizaki, and T. Fujita, Phys. Rev. Lett. 76, 3786 (1996).
- ¹¹ C. Bergemann, A. P. M ackenzie, S. R. Julian, D. Forsythe, and E. Ohm ichi, Adv. Phys. 52, 639 (2003).
- ¹² T. F. Smith, J. A. Mydosh, and E. P. Wohlfarth, Phys. Rev. Lett. 27, 1732 (1971).
- ¹³ M. Uhlarz, C. P. Eiderer, and S. M. Hayden, Phys. Rev. Lett. 93, 256404 (2004).
- ¹⁴ N. K imura, M. Endo, T. Ishiki, S. M inagawa, A. Ochiai, H. Aoki, T. Terashima, S. U ji, T. Matsumoto, and G. G. Lonzarich, Phys. Rev. Lett. 92, 197002 (2004).
- ¹⁵ A. J. Leggett, J. Phys. (Paris) 39, C 6 (1978).
- ¹⁶ C. P. Enz and B. T. M atthias, Science 201, 828 (1978).
- ¹⁷ D. Fay and J. Appel, Phys. Rev. B 20, 3705 (1979).
- ¹⁸ C. P. Eiderer, C. M. Uhlarz, S. M. Hayden, R. Vollmer, H. von Lohneysen, N. R. Bernhoeft, and G. G. Lonzarich, Nature (London) 412, 58 (2001).
- ¹⁹ E. A. Yelland, S. M. Hayden, S. J. C. Yates, C. P. Eiderer, M. Uhlarz, R. Vollmer, H. v. Lohneysen, N. R. Bernhoeft, R. P. Smith, S. S. Saxena, and N. K imura, cond-mat/0502341.
- ²⁰ R. P. Elliott, Constitution of Binary Alloys, First Supplement (McGraw-Hill, New York, 1965).
- ²¹ T. B. Massalski, J. L. Murray, L. H. Bennett, and H. Baker, Binary Alloy Phase Diagrams (American Society for Metals, Metals Park, OH, 1986).
- ²² L. W. M. Schreurs, H. M. W. eijers, A. P. J. V. Deursen, and A. R. De vroom en, Mat. Res. Bull. 24, 1141 (1989).
- ²³ A. P. J. van Deursen, L. W. M. Schreur, C. B. Admiraal, F. R. de Boer, and A. R. de Vroom en, J. Mag. Mag. Mat. 54-57, 1113 (1986).
- ²⁴ J. M. Ziman, Principles of the Theory of Solids (Cambridge University Press, Cambridge, UK, 1964).

- ²⁵ A. A. Abrikosov, L. P. Gorkov, and I. E. Dzyaloshinski, *Methods of quantum field theory in statistical physics* (Dover, New York, 1963).
- ²⁶ A. Carrington, C. Maroenat, F. Bouquet, D. Colson, A. Bertinotti, J. F. Manucco, and J. Hamann, *Phys. Rev. B* 55, R 8674 (1997).
- ²⁷ J. P. Shepherd, *Review Scientific Instruments* 56, 273 (1985).
- ²⁸ S. Ogawa and N. Sakamoto, *J. Phys. Soc. Jpn.* 22, 1214 (1967).
- ²⁹ G. S. Knapp, F. Fradin, and H. Culbert, *J. Appl. Phys.* 42, 1341 (1971).
- ³⁰ S. Ogawa, *J. Phys. Soc. Japan* 40, 1007 (1976).
- ³¹ P. Mattocks and D. Melville, *J. Phys. F: Metal Phys.* 8, 1291 (1978).
- ³² F. M. Grosche, C. P. Eiderer, G. J. McMullan, G. G. Lonzarich, and N. R. Bernhoeft, *Physica B* 206-207, 20 (1995).
- ³³ M. Seeger, H. Kronmüller, and H. J. Blythe, *J. Magn. Mater.* 139, 312 (1995).
- ³⁴ M. Uhlarz, C. P. Eiderer, and S. M. Hayden, *J. Magn. Mater.* 272-276, 242 (2004).
- ³⁵ M. Shimizu, *Proc. Phys. Soc.* 84, 397 (1964).
- ³⁶ M. Shimizu, *Proc. Phys. Soc.* 86, 147 (1965).
- ³⁷ J. M. Yeomans, *Statistical Mechanics of Phase Transitions* (Oxford University Press, Oxford, UK, 1992).
- ³⁸ P. M. Chaikin and T. C. Lubensky, *Principles of Condensed Matter Physics* (CUP, Cambridge, 1995).
- ³⁹ N. R. Bernhoeft, S. A. Law, G. G. Lonzarich, and D. M. Paul, *Phys. Scripta* 38, 191 (1988).
- ⁴⁰ M. B. Walker and K. V. Samokhin, *Phys. Rev. Lett.* 88, 207001 (2002).
- ⁴¹ G. W. Crabtree, *Phys. Rev. B* 16, 1117 (1977).
- ⁴² H. J. Williams, *Phys. Rev.* 52, 747 (1937).
- ⁴³ T. I. Sigfusson and G. G. Lonzarich, *Physica Scripta* 25, 720 (1982).
- ⁴⁴ J. J. M. Franse and G. de Vries, *Physics* 39, 477 (1968).
- ⁴⁵ H. Brooks, *Phys. Rev.* 58, 909 (1940).
- ⁴⁶ G. C. Fletcher, *Proc. Phys. Soc. Section A* 67, 505 (1954).
- ⁴⁷ N. D. Mathur, F. M. Grosche, S. R. Julian, I. R. Walker, D. M. Freye, R. K. W. Haselwimmer, and G. G. Lonzarich, *Nature* 394, 39 (1998).
- ⁴⁸ C. P. Eiderer, G. J. McMullan, S. R. Julian, and G. G. Lonzarich, *Phys. Rev. B* 55, 8330 (1997).
- ⁴⁹ M. J. Steiner, F. Beckers, P. G. Niklowitz, and G. G. Lonzarich, *Physica B* 329-333, 1079 (2003).
- ⁵⁰ M. E. Fisher and J. S. Langer, *Phys. Rev. Lett.* 20, 665 (1968).
- ⁵¹ J. Mathon, *Proc. Roy. Soc. A* 306, 355 (1968).
- ⁵² R. Viswanathan, *J. Phys. F: Metal Phys.* 4, L57 (1974).
- ⁵³ E. P. Wohlforth, *Physica* 91B, 305 (1977).
- ⁵⁴ K. Makoshi and T. Moriya, *J. Phys. Soc. Japan* 38, 10 (1975).
- ⁵⁵ P. Mohn and G. Hilscher, *Phys. Rev. B* 40, 9126 (1989).
- ⁵⁶ A. Ishigaki and T. Moriya, *J. Phys. Soc. Japan* 68, 3673 (1999).
- ⁵⁷ A. Ishigaki and T. Moriya, *J. Phys. Soc. Japan* 65, 376 (1996).
- ⁵⁸ Y. Takahashi and H. Nakano, *J. Phys.: Cond. Mat.* 16, 4505 (2004).